On inconsistency in frictional granular systems

Pierre Alart, Mathieu Renouf

On inconsistency in frictional granular systems

Pierre Alart · Mathieu Renouf

Abstract The numerical simulation of granular systems is often based on a discrete element method. The NonSmooth Contact Dynamics (NSCD) approach allows to solve a large range of granular problems, and specially involving rigid bodies. However we may face with difficulties for achieving successfully some simulations. The slow convergence of the nonsmooth solver may be attributed sometimes to a ill-conditioned system, but the convergence may also fail. The aim of the paper is first to identify the situations leading to the inconsistency of the mathematical problem to solve. Some simple granular systems are investigated in details. Related theoretical results are recalled and applied. A practical alternative is briefly analyzed and tested.

Keywords NonSmooth Contact Dynamics · Frictional granular media · Painlevé paradox

Mathematics Subject Classification (2000) 65L08 · 49J52 · 65L80

1 Motivation (based on numerical experiments)

The numerical simulation of complex dynamical systems is an important way for studying phenomena that are difficult to investigate experimentally. We could then speak about computational granular dynamics as a specific scientific field similarly to the computational fluid dynamics thirty years ago [5].

P. Alart
LMGC, Univ. Montpellier, CNRS, Montpellier, France
Laboratoire de Micromécanique et d'Intégrité des Structures (MIST), IRSN, CNRS, Université de Montpellier
Tel.: +33(0)4 67 14 39 89
Fax: +33(0)4 67 14 39 89
E-mail: Pierre.Alart@umontpellier.fr

M. Renouf
LMGC, Univ. Montpellier, CNRS, Montpellier, France

The numerical investigation progresses so quickly with respect with the experiments that the comparison between simulations and experiments is often rather coarse. Moreover the numerical tools may be used beyond their limits of validity because mathematical proofs are not available or are neglected. We propose to analyse the contributions, but mainly the conditions of use of the NonSmooth Contact Dynamics (NSCD) approach, developed by J.J. Moreau [21,23] and M. Jean [16], applied to the granular systems starting from some numerical experiments. The NSCD method has been developed for dealing with large collections of packed bodies and then for simulating the behaviour of granular materials. The Nonlinear Gauss-Seidel (NLGS) algorithm is the generic solver applied to the NSCD formulation. This combination allows simulation of the behaviour of a collection of (especially rigid) bodies involving different and mixed regimes: statics, slow dynamics (solid), fast dynamics (fluid). Numerous examples [31,34,19,18,36] illustrate the ability of the Moreau's approach for dealing with a large range of granular problems.
The present paper has been motivated by an homage to the contributions of J.J. Moreau, died in 2014, in the field of nonsmooth mechanics. These contributions at the end of his life concerned the numerical aspects and the applications focussed on the granular systems. J.J. Moreau wrote a single paper in a peer-reviewed journal on the theoretical foundations of the nonsmooth contact dynamics [21]. Thereafter he privileged the conferences, often as invited speaker, for promoting the NSCD approach through instructive numerical examples and sometimes some theoretical remarks. If the NSCD approach has been used by a large number of researchers, its theoretical foundations has been only investigated by few scientists and specially by B. Brogliato and his team [8,15,1]. The homage was then the occasion to deepen the study of some theoretical aspects of the NSCD approach in underlining the interest of the theory and in addressing the limits.
For illustrating the limits of the NSCD approach we focus our attention on dense granular systems that are strongly confined. In order to respect the elegant rusticity of the Moreau's approach we restrict the analysis to a collection of rigid bodies without considering global or local deformations of the grains. Some simple examples highlight the issue of inconsistencies, i.e. some configurations for which no solution exists, as well as indeterminacies, i.e. configurations that lead to non-uniqueness of solutions. We recover here the features of the Painlevé paradox underlined at the beginning of the twentieth century. The plurality of solutions has been numerically investigated by Moreau for an equilibrium and for a granular flow [25], but the inconsistency is only the subject of some remarks in some papers or conferences [24,25].
However the non existence of solutions is a more important challenge we have to face. Its occurence may compromise the use of the NSCD approach or at least suggest a precautionary principle. The main objective of the paper is to better identify the origins of the numerical difficulties inherent in the model proposed by the NSCD approach. The second goal is to propose a simple workaround to the problem of inconsistency. In Section 2, starting from a NSCD software and numerical experiments, we first identify the sit-

uations leading to this non existence among them the granular systems submitted to moving walls. Section 3 is dedicated to the analytical investigation of simple granular systems for illustrating the origins of non-existence and ill-conditioning. Some theoretical results are presented in Section 4 and are applied to the previous examples. Finally a practical alternative is developed in Section 5. We justify by this way the use of the Coulomb-Orowan frictional model as a numerical strategy of workaround, even if the shear threshold parameter is not available.

2 Nonsmooth contact dynamics of a collection of rigid bodies

2.1 Discrete-time contact problem with friction

The equations are directly presented according to a time-stepping integration scheme and with imposed velocities for some boundary bodies. The variables are summarized in Table 1. The multicontact system is restricted to a collection of rigid bodies. The possible configurations of the system are parametrized through the generalized coordinates of the free bodies, say x, from which derive the generalized velocities V. The dimension of x is the number of degrees of freedom. According to classical kinematic analysis the relative velocity v_α at some contact α is given by a relation $v_\alpha = H_\alpha^T V + G_\alpha^T V^*$, where H_α and G_α are connectivity mappings. V^* denote the prescribed velocities of some bodies, usually located at the boundary of the granular system. Based on duality considerations (conservation of the power expressed with local variables or generalized variables), the representative R_α of the local reaction impulse r_α for the generalized variable system satisfies the relation, $R_\alpha = H_\alpha r_\alpha$.

$[t^i, t^f]$	Time interval (initial / final instant, $dt = t^f - t^i$, time step)
x^i (resp. x for x^f)	Free generalized coordinates at time t^i (resp. t^f)
V^i (resp. V for V^f)	Free generalized velocities at time t^i (resp. t^f)
V^*	Prescribed velocities at time t^f
R^d	Given impulses over the time step
R	Contact impulses over the time step
g (for $g(x)$)	Normal contact gaps at contacts
v (for v^f)	Relative velocities at contacts
r	Contact forces or impulses at contacts
H (for $H(x)$)	Contact to grain linear mapping
H^T (for $H^T(x)$)	Grain to contact linear mapping
M (for $M(x)$)	Inertia matrix

Table 1 General notations

The connectivity mapping H depends implicitly on the generalized coordinates, but this dependency is omitted for convenience. Some kinematic variables are defined at the final instant t^f, but the exponent is suppressed for underlining that these variables are the unknowns as well as the contact

impulses over the time step. The fundamental equations are split into three classes and written in the following according to the global variables related to the bodies or to the contacts. For more details refer to [21,16].

Dynamics equation. The discretized equation of dynamics invokes the initial and final generalized velocities in the left-hand side and the given impulses R^d and the contact impulses R in the right-hand side. The contact impulse on a given body is provided by the covariant components of the impulses at all the contacts concerning the body via the admissibility equations, i.e. the integral over $[t^i, t^f]$ of the contact forces,

$$M\ (V\ -\ V^i)\ =\ R\ +\ R^d. \tag{1}$$

Admissibility equations. The connectivity mappings H and H^T links the generalized velocities to the relative velocities, and by duality the contact impulses between covariant and contravariant components,

$$\begin{cases} v\ =\ H^T\ V\ +\ G^T\ V^*\ =\ H^T\ V\ +\ v^*, \\ R\ =\ H\ r. \end{cases} \tag{2}$$

Contact behaviour. All the contact laws are formally represented by a relation between the local relative velocity v_α and the contact impulse r_α. Some parameters may be implied in this relation, like the gap, the cumulated sliding, the wear...

$$\mathcal{R}(v,r)\ =\ 0\ \ \Leftrightarrow\ \ \mathcal{R}(v_\alpha, r_\alpha)\ =\ 0, \alpha = 1, n_{contact} \tag{3}$$

For instance, the frictional contact law is summarized in the following relationships (g^α is the predicted gap, the impulse and the relative velocity are split into normal et tangential components),

$$\begin{cases} \text{if } g^\alpha > 0,\ r^\alpha = 0 \\ \text{if } g^\alpha = 0,\ 0 \le v_n^\alpha \perp r_n^\alpha \ge 0 \end{cases} \quad \text{and} \quad \begin{cases} \text{if } \|v_t^\alpha\| = 0,\ \|r_t^\alpha\| \le \mu r_n^\alpha \\ \text{if } \|v_t^\alpha\| \ne 0,\ r_t^\alpha = -\mu r_n v_t^\alpha / \|v_t^\alpha\| \end{cases} \tag{4}$$

The reduced dynamics condenses the linear equations (1) and (2) in the single equation,

$$W\ r\ -\ v\ =\ -\ v^d, \tag{5}$$

where $W := H^T\ M^{-1}\ H$ defines the *Delassus operator* and the right-hand side v^d is split into two parts,

$$v^d\ :=\ H^T(\ V^i\ +\ M^{-1}\ R^d)\ +\ v^*. \tag{6}$$

Finally the system to solve is composed of the linear reduced dynamics (5) and the frictional contact relationships (3),

$$\begin{cases} W\ r\ -\ v\ =\ -\ v^d \\ \mathcal{R}(v,r)\ =\ 0 \end{cases} \tag{7}$$

2.2 Nonsmoothness, indeterminacy and inconsistency

A first analysis of the system (7) leads to discriminate the sources of theoretical and numerical difficulties.

The second line of system (7) concentrates different forms of nonsmoothness. The *spatial nonsmoothness* refers to the geometrical conditions of interpenetration that are expressed as a set of inequalities. The forces (or impulses) involved for imposing the interpenetration are active or not according to the contact status; this leads so to an inequality applied to the force. The dry friction itself is expressed via a threshold for the tangential contact force and a multivalued relationships between the contact force and the sliding velocity; we can speak then about *nonsmoothness in law*. Finally, when we deal with rigid bodies, collisions may occur leading to velocity jumps reflecting a *temporal nonsmoothness*.

The first line of system (7) is the dynamics equation privileging the contact impulses as the main unknowns. Consequently this linear system may be ill-posed because the W matrix is often singular, specially for dense granular media. In a previous work [4] we focussed on the null space of W. We have proposed an algorithmic answer by reformulating the initial problem with regularization of the reduced dynamics, introduction of a multiplier and an additional equation imposing to the right-hand side $v - v^d$ to be orthogonal to the null space. We can relate to this formulation, an algorithm with two phases, a smooth prediction phase and a nonsmooth correction phase. We obtained mixed conclusions. The convergence may be drastically improved, but a drift of the interpenetration is observed. For eliminating this drift, an elastic prediction may be used, and in this case we recover the drawbacks of the molecular dynamic method as parasitic vibrational effects or very small time steps. Moreover this strategy does not resolve the lack of solution of course, when the right-hand side cannot check simultaneously the contact behavior (3) and the orthogonality to the null space. The inconsistency has to be specifically investigated.

Before starting a theoretical investigation, we underline a practical situation probably impacted by the inconsistency. The sandbox is an analogical device used by geophysicists to understand the folding of sedimentary layers due to the shortening. A numerical simulation of a sandbox device, based on a discrete element representation of the sand layers and the NSCD approach, has been performed some years ago (cf. Fig. 1). The simulation consists in moving the left vertical wall with a constant velocity to deform sand layers in view to reproduce tectonic motions. For simplicity only circular disks are considered for the full domain. A rigid contact model is chosen because the main part of the system is composed of weakly loaded particles, either static before the avalanche front on the right or flowing close to the sloped free surface. Only the corner zone on the left is submitted to a strong load due to the wall advance.

If elastic contacts were used in a molecular dynamics approach the time step size should be drastically reduced. Indeed, to perform an explicit simula-

tion controlled by the same final mean violation (i.e 1e-2 times the mean radius according to 16), the contact stiffness k should be approximatively equal to 2e9 N/m in regards of the force level in the left corner area. According to the classical equation used in a smooth Discrete Element Method to determine the time step size (i.e. $dtc = (1/N) * \sqrt{m/k}$, where m is the mass of a particle), such a stiffness value k leads to a time step size ranging from 1e-4 s to 2e-5 s according to the value of N (from 10 to 50 for reproducing at best a rebound). Now if we compare with the NSCD time step size (2.5e-2 s in our simulation), the ratio $dt(nonsmooth)/dt(smooth)$ range from 250 to 1250 approximatively. If in term of resolution, the resulting number of iterations is close (1000 nonsmooth iterations per step or 1 iteration per step in 1000 steps), we should proceed in the smooth case to a thousand contact detections in addition.

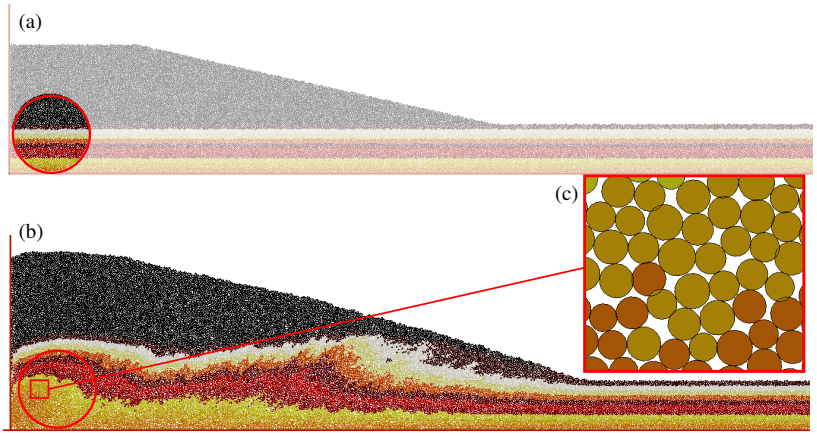

Fig. 1 Numerical sandbox device composed of 40 000 rigid circular particles: (a) initial state with a focus on the critical area; (b) final state and (c) zoom within the critical area at the end of the simulation.

The results have been analyzed in a previous paper [34] using the LMGC90 open source framework [12]. This simulation was one of the most difficult to achieve and it was performed again recently to investigate more deeply the numerical difficulties. The mechanical problem is characterized by a corner zone on the left that is strongly confined because it is submitted simultaneously to a high pressure of the accretionary wedge and to the moving wall. A zoom is performed on this region in Fig. 1 for underlining some parasitic interpenetrations between grains. The simulation of such complex granular systems presents some numerical convergence difficulties (cf. Fig. 2).

Indeed sometimes the nonsmooth solver does not converge for some time steps and reaches the prescribed maximal number of iteration (10^4 in the present case), but it converges again for the following time steps. Some plateaus may be even observed on the details of Fig. 15b. This strategy may be admissible if the errors, specially the interpenetrations, are not cumulated during

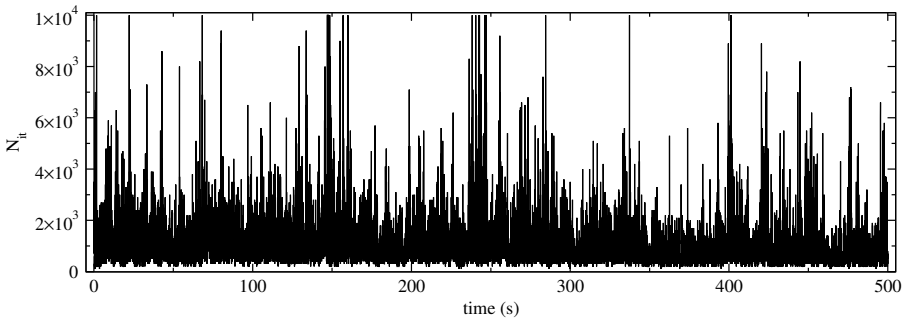

Fig. 2 Evolution of the iteration number during the simulation

the time steps. In favorable cases the strongly violated contacts at a certain moment may be released a few moments later. Only a post-treatment may validate the numerical strategy a posteriori. But such a situation is not satisfactory, even if it could be viewed as a self-correction type phenomenon. We will see in the next section that the residual interpenetration after a release stage may be sometimes large.

3 Inconsistency in simple granular systems

3.1 Detailed investigation of a simple problem

Let consider an elementary example with a single disk (ρ is its radius, m its mass, I its inertial moment equal to $\frac{m\rho^2}{2}$ for an homogeneous disk) in frictional contact with two obstacles as represented in Fig. 3. The disk is submitted to the

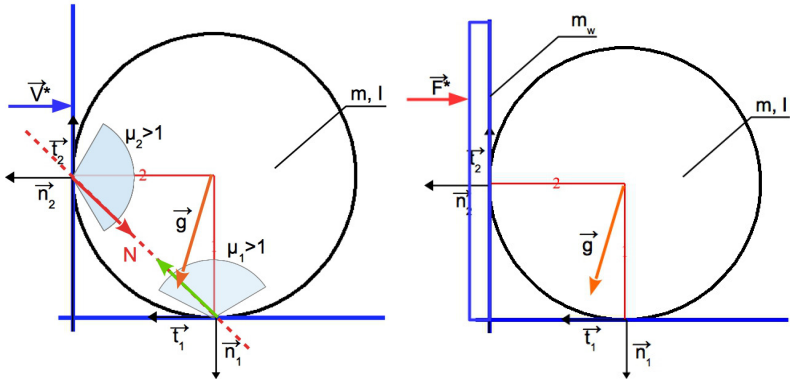

Fig. 3 A disk in a corner (the simplest example): velocity loading vs impulse loading

gravity in such away the left-side wall is not exactly vertical ($g_x < 0$ $g_y < 0$). The components of the initial velocity are equal to zero. So, with fixed walls,

the disk has to stay in the corner. But a velocity, $V^* > 0$, is prescribed to the vertical wall for pushing the disk. The dynamics is given by the equations,

$$\begin{cases} m(V_x - V_x^{init}) &= R_x + dt\ m\ g_x \\ m(V_y - V_y^{init}) &= R_y + dt\ m\ g_y \\ \frac{m\rho^2}{2}(\omega - \omega^{init}) &= R_\omega \end{cases} \tag{8}$$

The admissibility equation defining the relative velocities, $v = H^T V + v^*$, is then expanded as,

$$\begin{Bmatrix} v_n^1 \\ v_t^1 \\ v_n^2 \\ v_t^2 \end{Bmatrix} = \begin{bmatrix} 0 & 1 & 0 \\ 1 & 0 & \rho \\ 1 & 0 & 0 \\ 0 & -1 & \rho \end{bmatrix} \begin{Bmatrix} V_x \\ V_y \\ \omega \end{Bmatrix} + \begin{Bmatrix} 0 \\ 0 \\ -V^* \\ 0 \end{Bmatrix} \tag{9}$$

The reduced dynamics (expanded $\times \frac{1}{m}$) is then,

$$\underbrace{\begin{bmatrix} 1 & 0 & 0 & -1 \\ 0 & 3 & 1 & 2 \\ 0 & 1 & 1 & 0 \\ -1 & 2 & 0 & 3 \end{bmatrix}}_{W} \underbrace{\begin{Bmatrix} r_n^1 \\ r_t^1 \\ r_n^2 \\ r_t^2 \end{Bmatrix}}_{r} - \underbrace{\begin{Bmatrix} v_n^1 \\ v_t^1 \\ v_n^2 \\ v_t^2 \end{Bmatrix}}_{v} = \underbrace{\begin{Bmatrix} 0 \\ 0 \\ V^* \\ 0 \end{Bmatrix}}_{-v*} + dt \underbrace{\begin{Bmatrix} -g_y \\ -g_x \\ -g_x \\ g_y \end{Bmatrix}}_{H_f^T\ M^{-1}R^d} \tag{10}$$

The system to solve (7) is then *piecewise linear* in a two-dimension modeling, with eight unknowns (four impulse components and four relative velocity components) and sixteen regions of linearity corresponding to contact statuses deriving from the relationship (4). The global contact status is a couple of single status as reported on Table 2 : NC for Non Contact, A for Adherence, S_{ε_i} for Slip in the ε_i direction of the i^{th} contact ($\varepsilon_i = \pm 1$ forward/backward). The forthcoming analysis is based on the assumptions: $V^{init} = 0$, $\mu_1 > 1$, $\mu_2 > 1$. On Table 2 each linearity region, according to the contact status, provides, or not, a presumed solution. When an inequality is noted, the corresponding inequality defining a part the contact status is violated and the presumed solution is then invalidated. For example, in the first status, (NC, NC), in the table the normal relative velocity v_n^2 of the second contact has to be positive, but the presumed solution is negative according to the assumption $V^* > 0$. Mainly the solution is determined by neglecting the smooth part of the right-hand side by setting $dt = 0$. From a numerical point of view this consists in imposing a time step as small as possible. But for some statuses we can conclude only by taking into account the (force) external loading; the status is then indexed by a star like the second line in the table.

The five last statuses (the two last lines of Table 2) require a detailed investigation. The four sliding statuses are reported on Table 3 according to the sign of ε_1 and ε_2. The presumed solutions are invalidated because at least one admissibility inequality is not verified.

Table 2 Presumed solutions according to the contact status

Status	Presumed impulses	Presumed relative velocities
(NC, NC)	$\begin{Bmatrix} r_n^1 \\ r_t^1 \\ r_n^2 \\ r_t^2 \end{Bmatrix} = \begin{Bmatrix} 0 \\ 0 \\ 0 \\ 0 \end{Bmatrix}$	$\begin{Bmatrix} v_n^1 \\ v_t^1 \\ v_n^2 \\ v_t^2 \end{Bmatrix} = \begin{Bmatrix} 0 \\ 0 \\ -V^* < 0 \\ 0 \end{Bmatrix}$
$(NC, A)^*$	$\begin{Bmatrix} r_n^1 \\ r_t^1 \\ r_n^2 \\ r_t^2 \end{Bmatrix} = \begin{Bmatrix} 0 \\ 0 \\ -dtg_x + V^* \\ \frac{dt}{3} g_y \end{Bmatrix}$	$\begin{Bmatrix} v_n^1 \\ v_t^1 \\ v_n^2 \\ v_t^2 \end{Bmatrix} = \begin{Bmatrix} \frac{2dt}{3} g_y < 0 \\ V^* + \frac{2dt}{3} g_y \\ 0 \\ 0 \end{Bmatrix}$
(A, NC) *or* (S_{ε_1}, NC)	$\begin{Bmatrix} r_n^1 \\ r_t^1 \\ r_n^2 \\ r_t^2 \end{Bmatrix} = \begin{Bmatrix} 0 \\ 0 \\ 0 \\ 0 \end{Bmatrix}$	$\begin{Bmatrix} v_n^1 \\ v_t^1 \\ v_n^2 \\ v_t^2 \end{Bmatrix} = \begin{Bmatrix} 0 \\ 0 \\ -V^* < 0 \\ 0 \end{Bmatrix}$
(NC, S_{ε_2})	$\begin{Bmatrix} r_n^1 \\ r_t^1 \\ r_n^2 \\ r_t^2 \end{Bmatrix} = \begin{Bmatrix} 0 \\ 0 \\ V^* \\ \varepsilon_2 \mu_2 V^* \end{Bmatrix}$	$\begin{Bmatrix} v_n^1 \\ v_t^1 \\ v_n^2 \\ v_t^2 \end{Bmatrix} = \begin{Bmatrix} -\varepsilon_2 \mu_2 V^* \\ (2\varepsilon_2 \mu_2 + 1) V^* \\ 0 \\ 3\varepsilon_2 \mu_2 V^* > 0 \end{Bmatrix}$
(A, S_{ε_2})	$\begin{Bmatrix} r_n^1 \\ r_t^1 \\ r_n^2 \\ r_t^2 \end{Bmatrix} = \begin{Bmatrix} \frac{3}{2} \frac{\varepsilon_2 \mu_2 V^*}{1 - \varepsilon_2 \mu_2} < 0 \\ -\frac{1}{2} \frac{(1 + 2\varepsilon_2 \mu_2) V^*}{1 - \varepsilon_2 \mu_2} \\ \frac{3}{2} \frac{V^*}{1 - \varepsilon_2 \mu_2} \\ \frac{3}{2} \frac{\varepsilon_2 \mu_2 V^*}{1 - \varepsilon_2 \mu_2} \end{Bmatrix}$	$\begin{Bmatrix} v_n^1 \\ v_t^1 \\ v_n^2 \\ v_t^2 \end{Bmatrix} = \begin{Bmatrix} 0 \\ 0 \\ 0 \\ -V^* \end{Bmatrix}$
$(S_{\varepsilon_1}, A)^*$	$\begin{Bmatrix} r_n^1 \\ r_t^1 \\ r_n^2 \\ r_t^2 \end{Bmatrix} = \begin{Bmatrix} \frac{-dtg_y}{1 + \varepsilon_1 \mu_1} < 0 \ (\varepsilon_1 = -1) \\ \frac{-\varepsilon_1 \mu_1 dtg_y}{1 + \varepsilon_1 \mu_1} \\ \frac{\varepsilon_1 \mu_1 dtg_y}{1 + \varepsilon_1 \mu_1} - dtg_x + V^* \\ \frac{\varepsilon_1 \mu_1 dtg_y}{1 + \varepsilon_1 \mu_1} \end{Bmatrix}$	$\begin{Bmatrix} v_n^1 \\ v_t^1 \\ v_n^2 \\ v_t^2 \end{Bmatrix} = \begin{Bmatrix} 0 \\ V^* > 0 \ (\varepsilon_1 = +1) \\ 0 \\ 0 \end{Bmatrix}$
$(S_{\varepsilon_1}, S_{\varepsilon_2})$	$\begin{Bmatrix} r_n^1 \\ r_t^1 \\ r_n^2 \\ r_t^2 \end{Bmatrix} = \begin{Bmatrix} \frac{\varepsilon_2 \mu_2}{1 + \varepsilon_1 \varepsilon_2 \mu_1 \mu_2} V^* \\ \frac{\varepsilon_1 \varepsilon_2 \mu_1 \mu_2}{1 + \varepsilon_1 \varepsilon_2 \mu_1 \mu_2} V^* \\ \frac{1}{1 + \varepsilon_1 \varepsilon_2 \mu_1 \mu_2} V^* \\ \frac{\varepsilon_2 \mu_2}{1 + \varepsilon_1 \varepsilon_2 \mu_1 \mu_2} V^* \end{Bmatrix}$	$\begin{Bmatrix} v_n^1 \\ v_t^1 \\ v_n^2 \\ v_t^2 \end{Bmatrix} = \begin{Bmatrix} 0 \\ \frac{1 + 3\varepsilon_1 \varepsilon_2 \mu_1 \mu_2 + 2\varepsilon_2 \mu_2}{1 + \varepsilon_1 \varepsilon_2 \mu_1 \mu_2} V^* \\ 0 \\ \frac{2\varepsilon_2 \mu_2 (1 + \varepsilon_1 \mu_1)}{1 + \varepsilon_1 \varepsilon_2 \mu_1 \mu_2} V^* \end{Bmatrix}$
(A, A)	Indetermination or inconsistency	$v = 0$

Table 3 Sliding statuses and non admissible solutions

	$\varepsilon_1 = -1$	$\varepsilon_1 = +1$
$\varepsilon_2 = -1$	$r_n^1 < 0$	$r_n^2 < 0$
$\varepsilon_2 = +1$	$r_n^1 < 0$ $r_n^2 < 0$	$v_n^1 > 0$ $v_n^2 > 0$

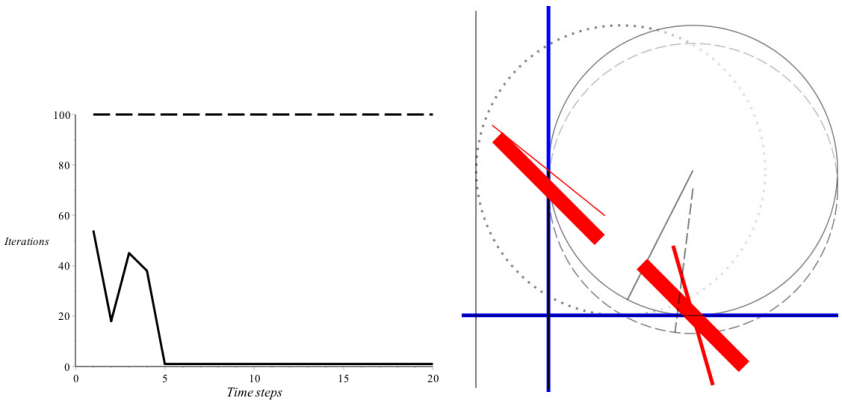

Fig. 4 Iteration evolution and final configuration for two cases: $\mu_1 = \mu_2 = 0.8$ (solid line), $\mu_1 = \mu_2 = 1.1$ (dashed line)

The status (A, A) provides an inconsistent system, $Wr = -v^d$, with an infinity of solutions (indetermination) for impulses if $V^* = 0$ and with no solution (inconsistency) if $V^* \neq 0$. Indeed, the null space of W is equal to the null space of the connectivity operator H. This kernel $Ker\ H$ is spanned by the vector $N = (1, -1, 1, 1)^T$. The existence of a solution (and then an infinity) requires that the right-hand side satisfies $N^T\ v^d = 0$. But $N^T\ v^d = N^T\ v^* = V^* \neq 0$.

From a numerical point of view an iterative solver, as the Gauss-Seidel algorithm, gives iterates $r^{(k)}$ close to the null space ($r \approx \gamma\ N$) whose the norm tends to infinity and satisfying the contact status (A, A) ($\mid r_t^1 \mid < \mu_1\ r_n^1$ and $\mid r_t^2 \mid < \mu_1\ r_n^2$) because $\mu_1 > 1$ and $\mu_2 > 1$. Then the iterates stay in the (A, A) region without converging.

The numerical tests confirm the previous analysis. Two choices of friction coefficients are studied: case 1 with $\mu_1 = \mu_2 = 0.8$ and case 2 with $\mu_1 = \mu_2 = 1.1$. For the second case the friction coefficients are above the critical value. The number of iterations is limited to a maximal value equal to 100. For the second case this maximal value is reached at each time step (dashed line in Fig. 4a). Fig. 4b shows the configuration of the system after 20 time steps; the initial position of the disk uses a dotted curve. The solid curve refers to the case 1 and the dashed curve to the case 2 where the interpenetration is obvious.

Controlling the moving wall with an impulse loading, instead of a velocity control, reveals not to be an alternative. In Fig. 3b the moving wall has a mass m_w and an impulse F^* is prescribed. The W matrix is then invertible because of an additional term $\lambda = \frac{m}{m_w}$,

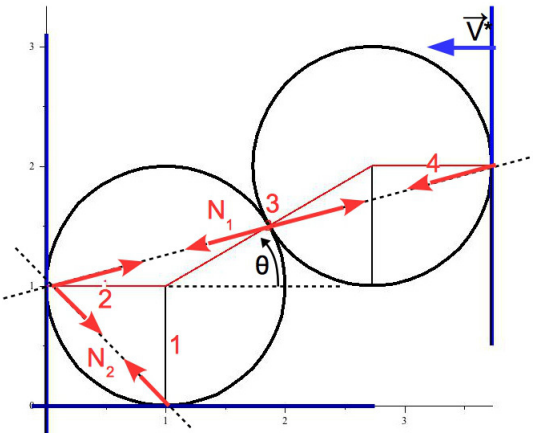

Fig. 5 Two disks in a box, four contacts and the two self-balanced impulses N_1 and N_2 (kernel of H)

$$W = \begin{bmatrix} 1 & 0 & 0 & -1 \\ 0 & 3 & 1 & 2 \\ 0 & 1 & 1+\lambda & 0 \\ -1 & 2 & 0 & 3 \end{bmatrix}. \tag{11}$$

Unfortunately the only solution of the system is no motion as great the magnitude of the prescribed impulse F^*.

3.2 Heuristic investigation of slightly more complex problems

The previous example suggests defining a critical friction coefficient beyond which the intersection of Coulomb cones and the null space is not reduced only to null vector. In the next example with 2 disks the null space is generated by two elements N_1 and N_2 represented in Fig. 5. The critical friction coefficient may be yet easily determined for each contact with respect to the θ angle, $\mu^1_{crit} = 1$, $\mu^{2,3,4}_{crit} = tan(\frac{\theta}{2})$. We restrict the study to a numerical investigation. We test a set of friction coefficients beyond the critical values: $\mu_1 = 1.3$ and $\mu^{2,3,4} = 0.28 > \mu^{2,3,4}_{crit} = tan(\frac{\pi}{12})$. We observe that the critical friction coefficient may be relatively small.

The simulation is performed with two versions of the algorithm. A first version of the NLGS algorithm does not use an initialization of the contact impulses; the impulse is reset to zero at each time step; it is called *without memory*. The second version, called *with memory*, initializes the impulses with the values obtained for the previous time step. The two versions provide different evolutions. In Fig. 6 the saturation of the iteration number to the prescribed maximal value (300) occurs for the two versions during the first 13 time steps corresponding to an increase of the normal impulse with memory (solid

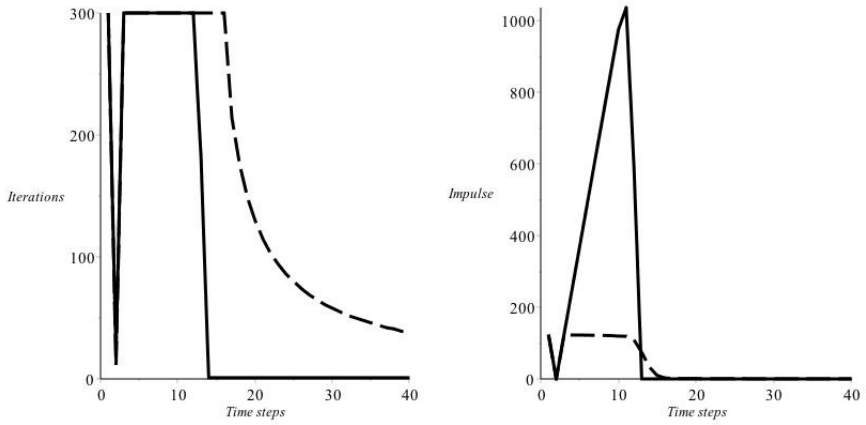

Fig. 6 Two disks in a box: evolution of the iterations and the normal impulse at the contact between the two disks - algorithms *without memory* (dashed line) and *with memory* (solid line)

line) and a stagnation without memory (dashed line). After this first stage the convergence is restored according to two different regimes: a fast convergence with memory, a slow convergence without memory. Such a behavior is easily explained by the evolution of the configuration in Fig. 7. During the first stage the θ angle increases until the friction coefficient becomes below the critical value. Without memory, the two disks stay in contact with a decreasing contact impulse, but with an important residual interpenetration. With memory, the contact impulse increases drastically until removal of the wedge leading to an artificial increase in the kinetic energy of the second disk (cf. the position of the disk at the final configuration).

Such behaviors allow to explain the analysis of the results on the sandbox simulation in Section 1. The temporary inconsistency of the system combined with an incomplete resolution may lead either to increasing parasitic interpenetrations, or to residual interpenetrations when the system becomes consistent again, or to an artificial kinetic energy restitution.

From a numerical point of view the existence of a null space is not the only drawback. In Fig. 8, with three disks, the self-balanced impulse network is geometrically localized in a corner; in fact a single disk is really confined; the system is globally "slack". Thus the algorithm converges even if the convergence is slow for the first time step with 1350 iterations for a stopping criterion similar to previous tests. The prescribed velocity of the moving wall does not solicit the self-balanced impulse network. The mathematical problem is not really ill-posed but only ill-conditioned. The first time step provides high magnitude impulses in the four first contacts leading to the loosening of the system for the next time steps as illustrated in Fig. 8.

Fig. 9 presents an other configuration with three disks and three walls leading to a jamming characterized by an impulse network increasing in the kernel of the H operator geometrically depicted on the figure. The system is

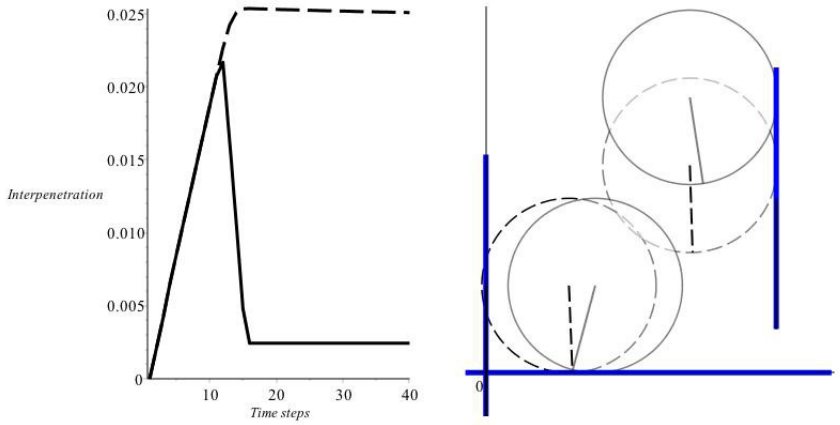

Fig. 7 Two disks in a box: evolution of the interpenetration and final configurations - algorithms *without memory* (dashed line) and *with memory* (solid line)

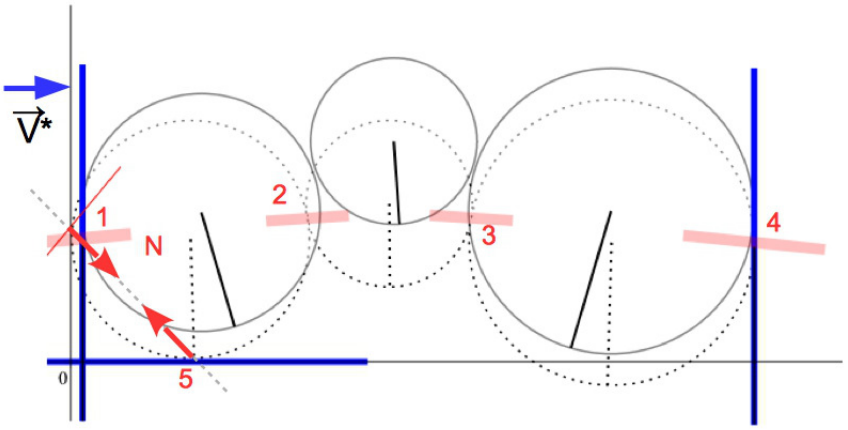

Fig. 8 Three disks in a box: "slack" system. Friction coefficients equal to 0.7. First time step configuration (dashed curves) with impulses at contacts (blurred), final configuration (solid curves).

globally "confined" and, contrary to the "slack" case, the self-balanced impulse network crosses the whole system; the problem is then inconsistent anew.

4 Related theoretical results and applications

The inconsistency in the dynamics of systems involving Coulomb friction was a matter of controversy during the first quarter of the twentieth century. It was observed that some initial value problems could admit several solutions or no solution and also that the behavior of the investigated system depended on its constants on a discontinuous way. At the time Painlevé [29] considered these

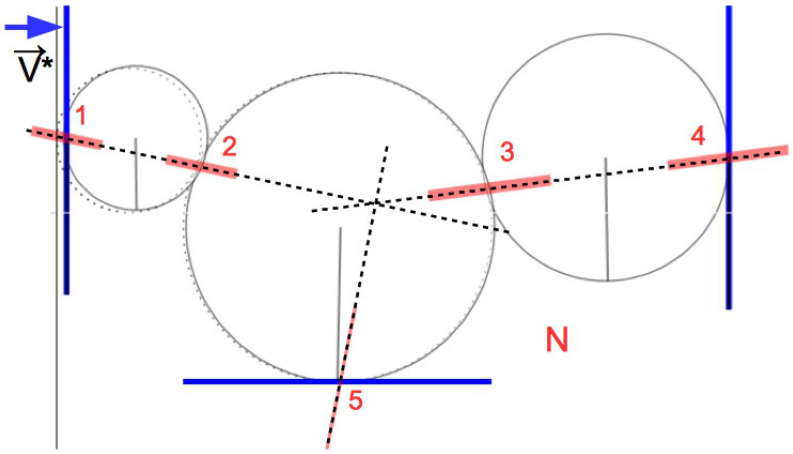

Fig. 9 Three disks in a box: "confined" system. Friction coefficients equal to 0.3. Jammed system with increasing impulses in the null space, no convergence and large interpenetrations.

findings as contradicting the very bases of Physics. This controversy is known as the *Painlevé paradoxes*, even if this expression is considered by Moreau [25] as a disquieting locution. Indeed, as mentioned initially by Lecornu [20], velocities jumps allow to escape from inconsistant configurations and the physical phenomenon is a dynamical analogue to the locking effect, well known in the statics of mechanisms with dry friction. The dynamic locking differs from the static locking because the magnitude of inertial forces tends to infinity. Dynamic locking, that Moreau proposes to call *frictional paroxysm*, is commonly observed in practice. The example of the chattering motion of a piece of chalk at an angle against a blackboard, so that a dotted line is drawn, was already put forward by Delassus [11] and numerically investigated by Moreau with a NSCD algorithm. More recently, Génot and Brogliato introduce, for this example, a critical friction coefficient below the contact forces of which remain bounded [15]. The literature about the *Painlevé paradoxes* is too vast to be reproduced here, but we can refer to a recent review paper [10]. Moreover all these analysis concern the formulation continuous in time for small size systems. For simple problems with a single body the locking may be resolved by a temporary enrichment of the model, taking into account elasticity for instance. Such a approach is not practicable for a large number of degree of freedom as in a granular system, for which the occurence of jamming may be very frequent and the discretization of deformable grains is computationally expensive. Moreover the elasticity of the grains does not allow to use the large time steps inherent to the NSCD approach. The time step has to be drastically reduced for reproducing the wave propagation.

The next section investigates the dynamical frictional problem in finite dimension with discretized time.

4.1 Existence theorems (about an old problem)

The above results consider the problem continuous in time. But we restrict our investigation to the problem on a single time step. The precursor work is due to Klarbring and Pang [17] on a static problem. From a mathematical point of view the system to solve (12) is similar to ours, constituted by the equations (1), (2) and (3). However the mass matrix M is replaced by the stiffness matrix K, and the velocities (generalized V and relative v) by the displacements (generalized u and relative v).

$$\begin{cases} K\ u\ =\ Hr\ +\ f \\ v\ =\ H^T u\ +\ v^* \\ \mathcal{R}(r,v)=0 \end{cases} \tag{12}$$

Using the present notation Acary et al [2] rewrite the existence assumption given by Klarbring and Pang [17] as reported in (13). The existence is guarantied if a scalar product implying f and v^* is non negative for all pair (u,r) satisfying some relations: rigid-body motion, self-balanced forces, admissibility condition without prescribed displacement and frictional contact behavior. This condition involves the data in term of the external force f and the prescribed displacement v^*.

$$\textit{Existence} \ \Leftarrow\ \left\{ \begin{matrix} f \\ v^* \end{matrix} \right\}^T \left\{ \begin{matrix} u \\ r \end{matrix} \right\} \geq 0\ \ \forall (u,r) / \begin{cases} K\ u\ =\ Hr\ =\ 0 \\ v\ =\ H^T u \\ \mathcal{R}(r,v)=0 \end{cases} \tag{13}$$

We can derive a result for the dynamical problem introduced at the beginning and rewritten in (14). We recover the mass matrix and the admissibility conditions in terms of velocities.

$$\begin{cases} M\ V\ =\ Hr\ +\ R^d\ +\ MV^i, \\ v\ =\ H^T V\ +\ v^*, \\ \mathcal{R}(r,v)=0 \end{cases} \tag{14}$$

Because the mass matrix is positive definite, the rigid-body motion is null. Thus the scalar product that we have to check non negative is reduced to v^* times r for all self-balanced forces r and zero relative velocities satisfying the frictional contact conditions. This condition is equivalent to v^* belongs to the dual cone to the intersection of the null space of H and the cartesian product of the Coulomb's cones denoted here L as noted in (15).

$$\textit{Existence} \ \Leftarrow\ v^{*T} r \geq 0\ \ \forall (0,r) / \begin{cases} Hr\ =\ 0 \\ \mathcal{R}(r,0)=0 \end{cases} \ \Leftrightarrow\ v^*\ \in\ (KerH \cap L)^* \tag{15}$$

Acary et al [2] proved a similar condition, without using a quasi-variational inequality formulation but the tools of the convex optimization. In the dynamical version, the external loading in term of impulse R^d, to compare with f in (12) is no more taken into account in the existence condition (15).

4.2 Application

It is instructive to apply the previous existence condition to the simple example of the section 3.1. In this case the null space is generated by the vector $k = (1, -1, 1, 1)^T$ representing the self-balanced impulses as drown in Fig. 3, i.e. two opposite vectors, $KerH = \{\lambda k \ ; \lambda \in \mathbb{R}\}$. If the friction coefficients μ_1 and μ_2 are greater than one (the corresponding cones are drawn in Fig. 3), the intersection $KerH \cap L$ is given by the positive half-space of the null space, $KerH \cap L = \{\lambda k \ ; \lambda \geq 0\}$. The dual cone is then defined as $(KerH \cap L)^* = \{w \in \mathbb{R}^4 \ ; k^T w \geq 0\}$. We have to check if the scalar product k times v^* is non negative. Using the expression given in (9), this scalar product is equal to $-V^*$. If the wall is pulled (if V^* is negative), the criterion is satisfied and the existence is assured. If the wall is pushed (if V^* is positive), the criterion is not satisfied and the existence is not assured. Let remark that this criterion does not take into account the external loading (here the gravity). Indeed, if we inverse the direction of the gravity, even if the criterion is not satisfied, a solution is possible.

5 A simple workaround

Acary and Cadoux propose in [3] an algorithm for checking the criterion computationally. This may be useful for large-scale problems. But if the criterion is not satisfied, what is the alternative to run the simulation? Moreover, even if the criterion is satisfied, the problem may be well-posed but ill-conditionned as underlined in Fig. 8 in section 3.2 and the computational time thus becomes prohibitive.

5.1 An enriched friction model: the Coulomb-Orowan law

From a mechanical point of view, when the contact impulses increase drastically, the whole model has to be revisited. A rigid model for the bodies is questionnable as soon as the grains are either sufficiently deformed or damaged. The deformation or damage may be global or local. However the elastic deformation is not a realistic response for a collection of hard grains like ballast stones for instance, for which the grain shape and the wear of the sharp corners is a more important phenomenon. Mathematically such a model enrichment does not seem to be an adequate solution for overcoming inconsistency or indetermination; Moreau in a conference dedicated to the plurality of solutions [22] remarks that "the occurrence of elasticity does not evade these difficulties". From a mechanical viewpoint, the fracture of grains is more relevant than the deformation of grain in the context of the dynamical behavior of a large collection of bodies. The fracture occurs at two levels.

At the macroscopic level, the grains may break in two or more parts. The description of such a phenomenon requires a sophisticated modeling. It would

have been necessary to start with non circular particles because the fracture will generate in any case non circular sub-particles. It may be based on a finite element method to describe the grain as a continuous medium; then a distribution of the elastic stress in the grains is available, and a cohesive zone model is performed to predict the decohesion zones [30]. In the context of a discrete element method, an other approach consists in computing the mean stress per rigid grain, in checking a fracture criterion per grain and in performing an heuristic fragmentation profile, according to the number of the contact points, leading to a decomposition of the grain into sub-grains [9]. In a variant the grains are discretized a priori into rigid subgrains and the fracture criterion is checked at all the internal interfaces [27]. Such strategies are expensive in implementation efforts and in term of computational time since it has to be coupled with the (nonsmooth) dynamics of a large collection of bodies.

At the microscopic level, i.e. at the contact area scale, the frictional contact law may be modified for accounting for the asperity flattening, the asperity fracture, or more generally a ploughing friction process. The simplest way is to consider the Orowan model [28], in which Coulomb law holds for low contact pressures on the one hand and the tangential friction stress is constant for high normal pressures on the other hand. In the same spirit, different models have been studied, specially for metal forming, by adding roughness contrast between contacting bodies [6] or a third body [35]... Here we adopt a simple Coulomb-Orowan model without smooth transition between the two regimes. The tangential forces are bounded by a Tresca type model for high pressures. An illustration is provided in Fig. 10 where the Coulomb cones are replaced by pen-type sets. Such a model requires the Tresca sliding threshold as a new parameter that characterizes the contact between particles in addition to the friction coefficient for the weak normal forces. This parameter may depend on several material and geometrical factors as the roughness and the curvature of the contacting surfaces. In any case it is not easy to identify this parameter for granular media; we cannot refer publicly to an industrial report which consists of an attempt for determining a friction law depending on the wear in ballast grains. In the following simple examples, the Tresca threshold is chosen without reference to a real value but only for testing the ability of the model to overcome the wedging processes.

5.2 Numerical experiments and acceleration attempts

First we apply the Coulomb-Orowan model to the simplest example. The improper interpenetration due to the inconsistency, observed in Fig. 4, is avoided as shown in Fig. 10. The Tresca threshold is activated for the second contact (impulse in grey on the figure). The convergence requires 18 iterations for the first time step, 6 for the second step and a single iteration for the following steps.

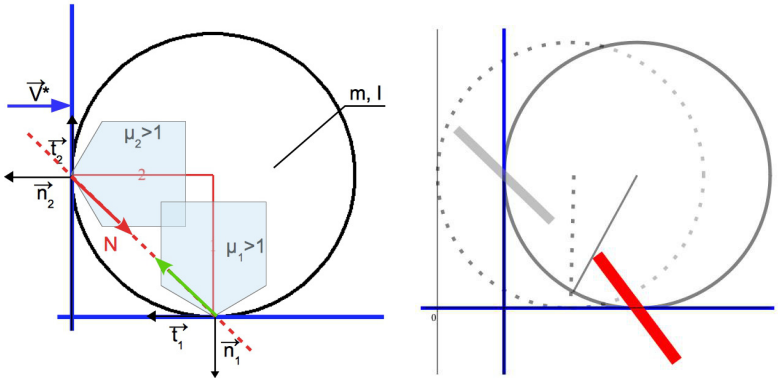

Fig. 10 A disk in a corner with pen-type sets (Coulomb-Orowan law) and final configuration (saturated threshold at the second contact in grey)

The Coulomb-Orowan model is then applied to the "confined" system with three disks. The wedging process, illustrated in Fig. 9, is again overcome as shown in Fig. 11. The saturation of the Tresca threshold is reached at the two first contact on the smallest disk. The convergence requires 173 iterations for the first time step, around 40 for the following steps.

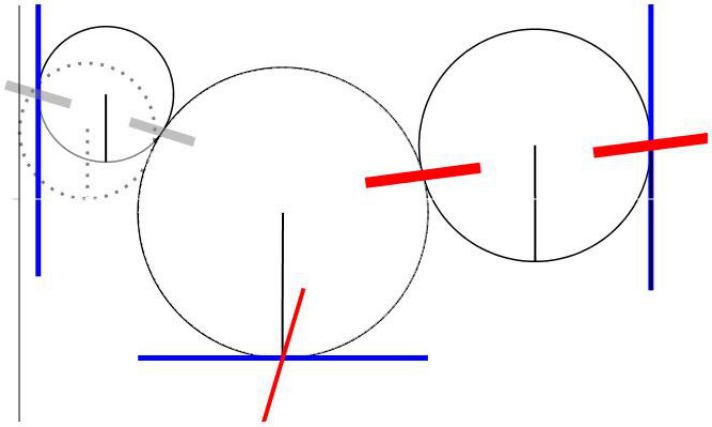

Fig. 11 Three disks in a box ("confined" system). Initial and final configurations with the Coulomb-Orowan law (saturated threshold at the two first contacts in grey)

The evolution of the impulse iterates for the first step is given in Fig. 12. The slow convergence is typical of the Gauss-Seidel algorithm. However the previous theoretical analysis of Section 4 suggests that the impulse iterates evolve close to the null space of the H operator; this is confirmed by the iterate trajectories until some trajectories cross the boundary of the pen-type set when the Tresca threshold is reached. Acceleration procedures may be derived from this remark. Without giving details the procedure consists of

three steps: first detecting the alignment of the iterates with the kernel of H, then determining the intersection with the pen-type set, finally jumping to this point and starting agin from this one. Two versions have been carried out. The global acceleration procedure detects the alignment on the full system. The local acceleration procedure performs this detection contact per contact using the projection of the null space on the subspace of the impulses of the current contact.

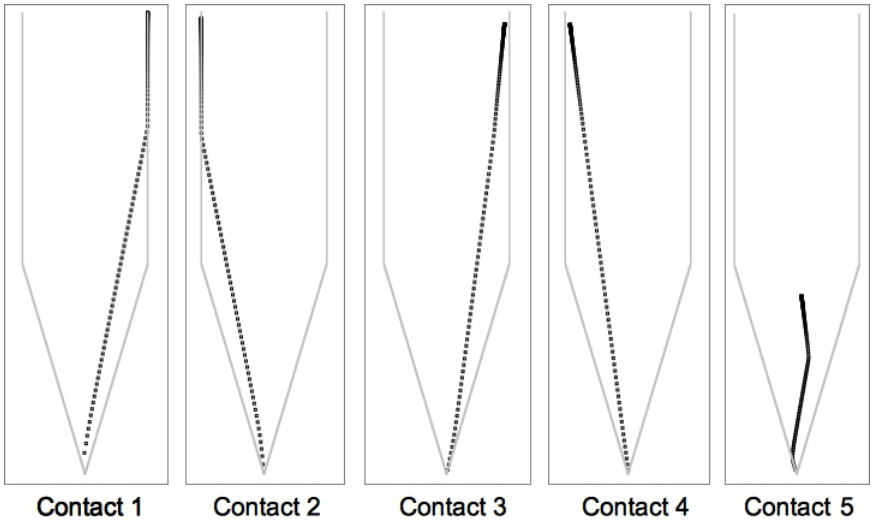

Fig. 12 Three disks in a box ("confined" system). Evolution of the impulse iterates at each contact.

Fig. 13 shows the implementation of these procedures on the confined system with three disks for the first contact. The iteration number decreases with these acceleration procedures, but the decrease is not so important because once the procedure is activated, the convergence rate of the Gauss-Seidel algorithm is recovered. In other words the acceleration is provisory. For more complex systems the acceleration procedures perturb the algorithm leading to the divergence. This explains that the details of the procedures are not given.

5.3 Return on the sandbox simulation

Finally, the Coulomb-Orowan model is applied to the sandbox system and compared to the solution obtained with the classical Coulomb friction model. The Coulomb friction coefficient is equal to 0.7.

The Tresca threshold is applied on the normal component of the contact force and is expressed in Newton. Two different values have been used: 10^4 N and 10^6 N. The higher value corresponds to the mean value of the contact force within the sample.

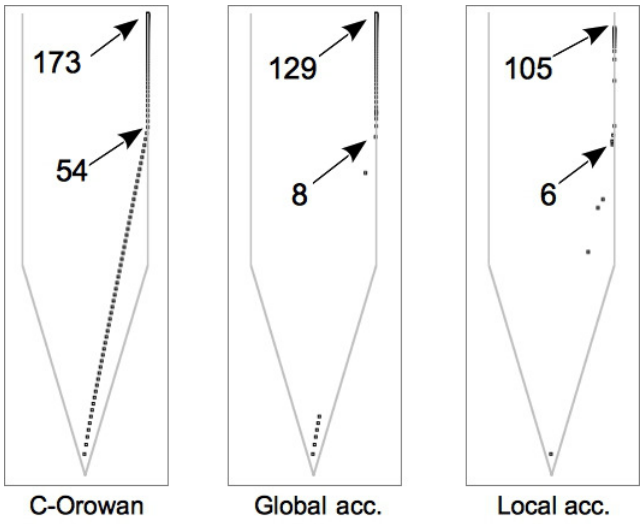

Fig. 13 Three disks in a box ("confined" system). Evolution of the impulse iterates at contact 1 with Coulomb-Orowan, the global acceleration and the local acceleration.

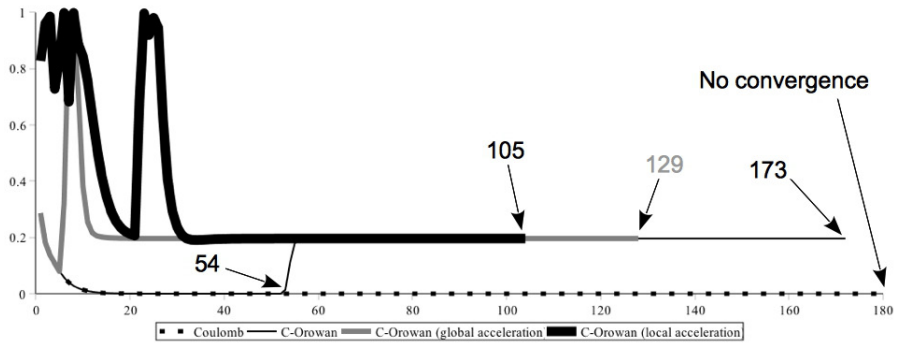

Fig. 14 Three disks in a box ("confined" system). Gap between the iterate trajectory and the null space with Coulomb, Coulomb-Orowan, the global acceleration and the local acceleration.

Figure 15a presents the evolution of the number of iterations obtained with the Coulomb and the Coulomb-Orowan models. During the simulation process using the Coulomb friction model, the algorithm reaches several times the prescribed number of iterations (fixed here to 10^4). This value are reached also during consecutive time steps as shown by the plateaus in Fig.15b. When the Coulomb-Orowan friction model is used, a different behavior is observed. For the higher threshold value, the maximal number of iterations is reached at the first step only. Then, the convergence is better on the whole process: the mean number of iterations is equal to 325 (in comparison with around 1 000 iterations for the Coulomb model). For the smaller threshold value, the maximal number of iterations is never reached and the mean number of iterations is equal to 110.

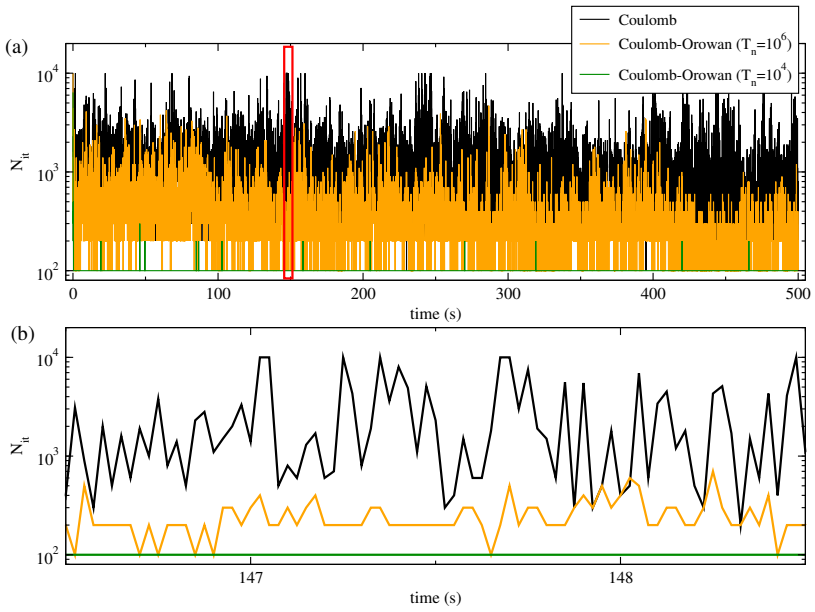

Fig. 15 Comparison of the evolution of iteration number (semilogarithmic representation) obtained for simulation using Coulomb friction and Coulomb-Orowan friction with two different thresholds (10^4 and 10^6).

Thus, as observed in the previous simple numerical experiments, the Coulomb-Orowan friction model can improve the convergence of the algorithm.

In complement of previous observations, the evolution of the mean violation is checked. Rather than to observe such an evolution on the whole system, an attention is given on the corner region close to the moving wall defined in Fig. 1a. Results are illustrated in Fig. 16a. They show that the mean violation increases for the three simulations. The mean violation value is quasi-equivalent for the Coulomb friction and the Coulomb-Orowan friction with a high threshold. It is reduced by a half for the Coulomb-Orowan friction with a low threshold.

Indeed, this reduction of the mean violation leads to some variation in the system properties. Figure 16b presents the contact force distribution (or pdf function [31]) within the system. It appears that the pdf function obtained with the Coulomb-Orowan friction with a low threshold is different of the two others friction models.

To summarize, the Coulomb-Orowan friction requires much less iterations than the Coulomb model. The mean violation is not reduced with a convergence criterion expressed in term of averaged quantities [16]. But it may influence the global mechanical properties of the considered system. If an experimental value of a Tresca threshold is not available, the mean value of the contact force seems a relevant value to define the Tresca threshold used in the Coulomb-Orowan model. Certainly such a recommendation is based on a first

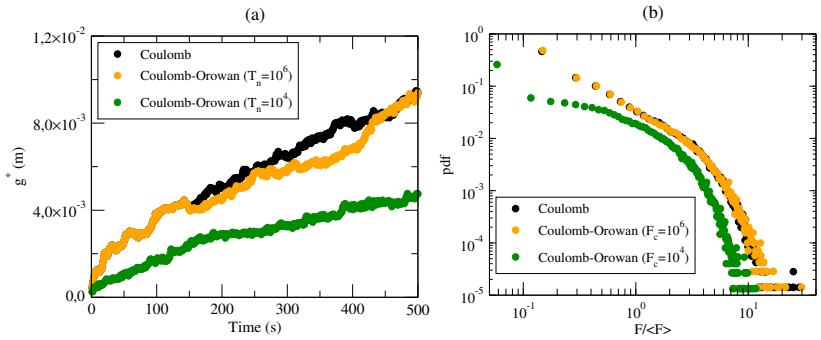

Fig. 16 (a) Evolution of the mean violation and (b) contact force distribution for the Coulomb and the Coulomb-Orowan models.

analysis on one confined system, but this seems to be pertinent because, as shown in [31], the mean value of the contact force separates the weak contact network and the strong contact network. The strong contacts concentrate the large normal forces dealing with the interpenetration and constitute the "load-bearing" network as underlined in [32].

6 Conclusion

The occurence of inconsistency of the modelling has been identified in granular systems and illustrated on simple examples. A theoretical direct investigation has been performed on these examples and a link between the kernel of the Delassus operator and the cartesian product of the Coulomb cones provides an existence theorem.
The Coulomb-Orowan friction model constitutes a practical alternative to the classical Coulomb law and a simple workaround to the non existence problem. It was tested on simple examples for overcoming the inconsistency. The relevancy of such a approach as a numerical remedy has been investigated on a sandbox process. The numerical results prove that the convergence is restored at each time step and the convergence rate is significantly improved. We can even give a recommendation for choosing a pertinent Tresca threshold when such a parameter is not experimentally available. However we are not theoretically sure that the inconsistency of the problem is always avoided. We need a theoretical study providing an existence theorem in this case. Moreover the Coulomb-Orowan model is not a remedy to the ill-conditioning. The ill-conditioning of a non smooth system of equations and inequations is difficult to quantify. The linear part of the system, given by the Delassus operator W, is commonly very ill-conditioned because this operator is singular, i.e. its condition number is infinite. Even if the null space of W is not solicited by the solution impulse network, as in the example of Fig. 8, the convergence may be very slow.
The attempt of acceleration procedures is not conclusive. This fact confirms

the difficulty to improve the convergence of iterative solvers on nonsmooth systems as reported in [33] for conjugate gradient type methods or in [36] for domain decomposition strategies. The ill-conditioning of such non smooth systems proves to be a very difficult topic.
The Coulomb-Orowan model leads to a smoother evolution of the contact impulse network. The relaxation of the wedging effects erases the possible dynamic crises observed in granular packings. Indeed such crises are revealed by acoustic emissions in some experiments. The simulation of such dynamic effects requires to add an elastic behavior of the grains or at least a restitution coefficient at the impacts. The notion of formal velocity proposed by Moreau, as a convex combination of the left velocity and the right velocity, allows to reproduce binary shocks, from inelastic to perfectly elastic shocks. But it is not able to simulate the propagation of shocks generated by elastic waves in a collection of rigid bodies with simultaneous multiple contacts. Some attempts of modeling the collisions of several rigid bodies lead to complex models difficult to identify [13,14] or restricted to simple systems as granular chains [26]. Such a topic is a forecoming challenge.

References

1. V. Acary and B. Brogliato, Numerical methods for nonsmooth dynamical systems: applications in mechanics and electronics, Springer Science & Business Media, (2008)
2. V. Acary, F. Cadoux, C. Lemaréchal and J. Malick, A formulation of the linear discrete Coulomb friction problem via convex optimization, Zeitschrift für angewandte Mathematik und Mechanik, 91(2), 155–175 (2011)
3. V. Acary and F. Cadoux, Applications of an existence result for the Coulomb friction problem, Recent Advances in Contact Mechanics, Springer, 45–66 (2013)
4. P. Alart, How to overcome indetermination and interpenetration in granular systems via nonsmooth contact dynamics. An exploratory investigation, Computer Methods in Applied Mechanics and Engineering, 270, 37–56, (2014)
5. J.D. Anderson and J. Wendt, Computational fluid dynamics, 334. Springer, (1995)
6. B. Avitzur and Y. Nakamura, Analytical determination of friction resistance as a function of normal load and geometry of surface irregularities, Wear, 107(4), 367–383 (1986)
7. E. Azéma and F. Radjai and G. Saussine, Quasistatic rheology, force transmission and fabric properties of a packing of irregular polyhedral particles, Mechanics of Materials, 41(6), 729–741, (2009)
8. B. Brogliato, Nonsmooth mechanics, Springer, (1999)
9. D. Cantor, N. Estrada, E. Azéma, Split-Cell Method for grain fragmentation, Computers and Geotechnics, 67, 150–156 (2015)
10. A.R. Champneys and P.L. Varkonyi, The Painlevé paradox in contact mechanics, arXiv preprint arXiv:1601.03545, (2016)
11. E. Delassus, Sur les lois du frottement de glissement, Bulletin de la Société Mathématique de France, 51, 22–33 (1923)
12. F. Dubois and M. Jean, The non smooth contact dynamic method: recent LMGC90 software developments and application. In Analysis and simulation of contact problems, 375–378, Springer Berlin Heidelberg (2006)
13. M. Frémond, Non-Smooth Thermodynamics, 480 pages, Springer (2002)
14. M. Frémond, Collisions, 282 pages, Universitá di Roma Tor Vergata, Dipartemento di Ingeneria Civile (2007)
15. F. Génot, B. Brogliato, New results on Painlevé paradoxes, European Journal of Mechanics - A/Solids, 18 (4), 653 – 677 (1999)

16. M. Jean, The non-smooth contact dynamics method, Computer Methods in Applied Mechanics and Engineering, 177, 235–257 (1999)
17. A. Klarbring and J-S. Pang, Existence of solutions to discrete semicoercive frictional contact problems, SIAM Journal on Optimization, 8(2), 414–442 (1998)
18. T. Koziara and N. Bićanić, A distributed memory parallel multibody contact dynamics code, International Journal for Numerical Methods in Engineering, 87(1-5), 437–456, (2011)
19. R. Laniel, P. Alart and S. Pagano, Discrete element investigations of wire-reinforced geomaterial in a three-dimensional modeling, Computational Mechanics, 42(1),67–76, (2008)
20. L. Lecornu, Sur la loi de Coulomb, Comptes Rendus Acad. Sci. Paris, 140, 847–848 (1905)
21. J. J. Moreau, Numerical aspects of sweeping process, Computer Methods in Applied Mechanics and Engineering, 177, 329–349 (1999)
22. J. J. Moreau, Modélisation et simulation de matériaux granulaires, in: Actes du 35eme Congres National dAnalyse Numérique (2003)
23. J. J. Moreau, An introduction to unilateral dynamics, in: Novel approaches in Civil Engineering (eds M. Fremond and F. Maceri), Lecture Notes in Applied and Computational Mechanics, Vol. 14, Springer-Verlag, pp. 1–46 (2004)
24. J. J. Moreau, Indetermination in the numerical simulation of granular systems, in: Powders and Grains 2005 (eds Garcia-Rojo, R., Herrmann, H.J. and Mc Namar, S.), Balkema, Leiden, pp. 109–112 (2005)
25. J. J. Moreau, Facing the plurality of solutions in non smooth mechanics, in: Nonsmooth/Nonconvex Mechanics with Applications in Engineering, Editions Ziti, Thessaloniki, 2006, pp. 3–12, proc. Internat. Conference in Memoriam of P. D. Panagiotopoulos.
26. N.S. Nguyen and B. Brogliato, Multiple impacts in dissipative granular chains, Lecture Notes in Applied and Computational Mechanics 72, Springer, (2014)
27. D.-H.Nguyen, E. Azéma, P. Sornay, F. Radjai, Bonded-cell model for particle fracture, Phys. Rev. E 91, 022203 (2015)
28. E. Orowan, The calculation of roll pressure in hot and cold flat rolling, Proceedings of the Institution of Mechanical Engineers, 150(1), 140–167 (1943)
29. P. Painlevé, Sur les lois de frottement et de glissement, Comptes Rendus Acad. Sci. Paris, 121, 112–115 (1905)
30. F. Perales, F. Dubois, Y. Monerie, B. Piar and L. Stainier, A NonSmooth Contact Dynamics-based multi-domain solver: Code coupling (Xper) and application to fracture, European Journal of Computational Mechanics/Revue Européenne de Mécanique Numérique, 19(4), 389–417 (2010)
31. F. Radjaï, M. Jean, J. J. Moreau, and S. Roux, Force distributions in dense two dimensional granular systems, Physical Review Letters, 77, 274–277 (1996)
32. F. Radjaï, D.E. Wolf, M. Jean, J. J. Moreau, Bimodal Character of Stress Transmission in Granular Packings, Physical Review Letters, 80(1), 61–64 (1998)
33. M. Renouf and P. Alart, Conjugate gradient type algorithms for frictional multi-contact problems: applications to granular materials, Computer Methods in Applied Mechanics and Engineering, 194(18-20), 2019–2041 (2005)
34. M. Renouf, F. Dubois, P. Alart, Numerical investigations of fault propagation and forced-fold using a non smooth discrete element method, European Journal of Computational Mechanics, 15, 549–570, (2006).
35. S. Stupkiewicz, S and Z. Mróz, A model of third body abrasive friction and wear in hot metal forming, Wear, 231(1), 124–138 (1999)
36. V. Visseq, A. Martin, D. Iceta, E. Azema, D. Dureisseix, and P. Alart, Dense granular dynamics analysis by a domain decomposition approach, Computational Mechanics, 49, 709–723 (2012)